

DYNAMICS OF POINT JOSEPHSON JUNCTIONS IN A MICROSTRIP LINE

J.-G. CAPUTO* AND L. LOUKITCH*

Abstract. We analyze a new long wave model describing the electrodynamics of an array of point Josephson junctions in a superconducting cavity. It consists in a wave equation with Dirac delta function sine nonlinearities. We introduce an adapted spectral problem whose spectrum gives the resonances in the current-voltage characteristic curve of any array. Using the associated inner product and eigenmodes, we establish that at the resonances the solution is described by two simple ordinary differential equations.

Key words. Josephson junctions, Dirac distribution, sine Gordon, current voltage characteristic spectral problem, resonance

AMS subject classifications. 35Qxx, 46Fxx, 35Pxx

1. Introduction. The macroscopic state of a superconductor is described by a complex field the order parameter. For low T_c superconductors it can be assumed that only the phase of the order parameter varies. The coupling of two such superconductors across a thin oxide layer is described by the Josephson equations [1].

$$(1.1) \quad V = \frac{d\Phi}{dt}, \quad I = sJ_c \sin\left(\frac{\Phi}{\Phi_0}\right),$$

where Φ is the phase difference between the top and bottom superconductor, V and I are, respectively, the voltage and current across the barrier, s is the contact surface, J_c is the critical current density and $\Phi_0 = \hbar/2e$ is the reduced flux quantum. These two Josephson relations together with Maxwell's equations imply the modulation of DC current by an external magnetic field in the static regime and the conversion of AC current into microwave radiation [2, 3]. Such Josephson junctions are then unique electronic systems for applications like the detection of magnetic fields, ultra fast electronics[3] and microwave sources and signal mixers [4],[5].

For the applications the devices are often associated to form arrays. The junctions can be in parallel or in series. The series arrays can lead to synchronization[6]. and deliver more output power for some applications. Their description is however more complex and we will not consider it here. Parallel arrays where the junctions are embedded between two superconducting planes are now relatively easy to prepare and the junction is protected from the atmosphere. In addition one can easily prepare an array with junctions of specific sizes and positions. Such non uniform arrays have been produced and analyzed in particular by Salez and co-workers at the Observatory of Paris. For these systems, the phase difference Φ satisfies an inhomogeneous 2D damped driven sine Gordon equation [7] resulting from Maxwell's equations and the Josephson constitutive relations (1.1). The damping is due to the normal electrons and the driving through the boundary conditions with an external current or magnetic field applied to the device.

To model such arrays authors have used lumped models where the spatial dependence between the junctions is omitted. This obliterates the wave features of the

*LABORATOIRE DE MATHÉMATIQUES, INSA DE ROUEN, B.P. 8, AVENUE DE L'UNIVERSITE 76801 SAINT-ETIENNE DU ROUVRAY, FRANCE. E-MAIL: CAPUTO@INSA-ROUEN.FR, LOUKITCH@INSA-ROUEN.FR

solution and does not describe well the experiments. Solving numerically the full two dimensional problem is of course possible, however it does not lead to understand simply the role of the parameters. Similar difficulties occur with global (hard) analysis. Consider for example the problem of finding the maximum current giving a static solution for a given magnetic field. Using such global analysis we obtained bounds [8] on the gradient of the solution that were independent of the area of the junctions so that little information could be obtained from them. To overcome these difficulties we recently introduced a continuous/discrete model that preserves the continuity of the phase and its normal gradient across the junction interface and where the phase is assumed constant in the junctions. The relative simplicity of the model allowed an unprecedented understanding of the static problem[9] and gave excellent agreement with the complex static response of the array[10]. Additionally the model allows to solve the inverse problem of building a device that produces a given static behavior[11].

The dynamic behavior of Josephson junctions is characterized by the current-voltage (I-V) characteristic curve. To understand this one needs to analyze periodic solutions of the problem. For a homogeneous long junction Kulik[12] developed a formalism using a high voltage ansatz and obtained average equations describing the I-V curve. This approach was extended by Cirillo et al [13] who showed that a magnetic field Γ reinforces the cavity modes such that $\Gamma = n\pi/l$. Using this approach these authors obtained excellent quantitative agreement with their experimental results. For arrays of equidistant junctions, a recent study by Pfeiffer et al[14] analyzed the fine features of the first resonant step in terms of Cerenkov radiation between a sine-Gordon discrete kink (fluxon) and a cavity mode. For one junction in a cavity, our theoretical study [15] revealed that the junction could stop waves across the cavity or enhance them throughout. We also found kink like solutions for the problem [19] and explained some features of the current-voltage characteristics. Here we analyze theoretically and numerically the model in particular when there is a capacity mismatch between the junctions and the cavity. This capacity ratio is usually large in experiments because the oxide layer in the junction is about 10 Angstroms while it is about 0.2 Micron in the strip. Taking this miss-match into account we introduce an associated linear problem which enables us to predict the position of the resonances in the current-voltage curve for any array. This linear problem defines eigenvalues and eigenmodes orthogonal with respect to an inner product that we establish. At these resonances the solution just contains the Goldstone mode and the corresponding eigenmode so the dynamics is described by two simple amplitude equations that we present and analyze.

The article is organized as such. After introducing the model in section 2, we analyze it in section 3, establish the periodicity of the current voltage curve as a function of the magnetic field and simplify the model using the time averaged (high voltage) solution. The resonances are studied in section 4 where we define the appropriate spectral problem for any given array and find its spectrum and associated inner product. Using the latter we analyze numerically the current voltage curves in section 5. In particular we establish and analyze the amplitude equations describing the system at resonance and discuss the situation for arrays containing many junctions.

2. The model.

2.1. The 2D problem. The device we model (see Fig.2.1) is composed of two overlapping superconducting layers, in which stand small¹ Josephson junctions. Using

¹compared to the Josephson coherence length λ_J

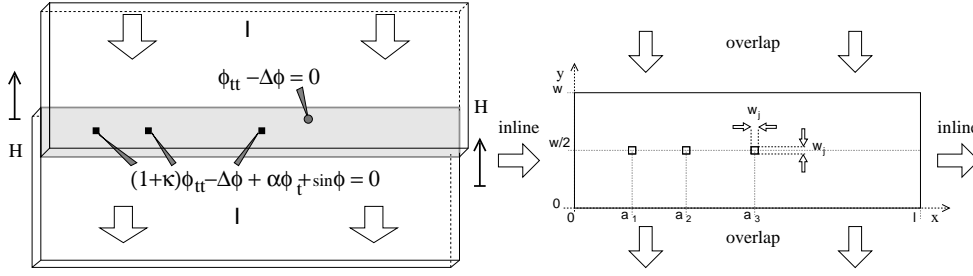


FIG. 2.1. The left panel shows the top view of a superconducting microstrip line containing three Josephson junctions. The parameters H, I and ϕ are respectively the applied magnetic field, the current and the phase difference between the two superconducting layers. The right panel shows the associated 2D domain of size $l \times w$ containing $n = 3$ junctions placed at the positions $y = w/2$ and $x = a_i, i = 1, n$.

the Josephson constitutive equations (eq.1.1) and Maxwell's equation, one obtains the following inhomogeneous sine-Gordon equation for Φ in the junction region Ω_j [2, 3]

$$(2.1) \quad C_j \Phi_{tt} - \frac{1}{L} \Delta \Phi + J_c \sin \left(\frac{\Phi}{\Phi_0} \right) + \frac{1}{R} \Phi_t = 0 ,$$

where C_j is the capacity of the junction per unit area, R the resistance per unit area due to normal electrons. The branch inductance $L = \mu_0 d_0$ involves the magnetic thickness d_0 , a quantity used by experimentalists. In the microstrip $\Omega - \Omega_j$, the Josephson and quasi-particle currents are absent so one obtains the wave equation,

$$(2.2) \quad C_l \Phi_{tt} - \frac{1}{L_l} \Delta \Phi = 0 ,$$

where the l subscripts indicate that we are in the linear region (i.e.: outside the junction). For inhomogeneous circuits like the one of Fig. 2.1 these two equations can be written as [15, 16]

$$(2.3) \quad C_l \Phi_{tt} - \nabla \left(\frac{1}{L(x)} \nabla \Phi \right) + g(x, y) \left[(C_j - C_l) \Phi_{tt} + J_c \sin \left(\frac{\Phi}{\Phi_0} \right) + \frac{\Phi_t}{R} \right] = 0 ,$$

where $g = 1$ in the junctions and 0 outside. This formulation guarantees the continuity of the phase and its normal gradient across the interfaces. At this point we will assume the same surface inductance L in the junctions and linear region. This simplifies greatly the formulation and can be realized in practical situations. To normalize the equation, we introduce the units of length and time, respectively the Josephson length λ_J and plasma frequency ω_p

$$(2.4) \quad \lambda_J = \sqrt{\frac{\Phi_0}{J_c L_l}} , \quad \frac{1}{\omega_p} = \sqrt{\frac{C_l \Phi_0}{J_c}} .$$

Finally we normalize space, time and phase as

$$(2.5) \quad \tilde{x} = x/\lambda_J, \quad \tilde{y} = y/\lambda_J, \quad \tilde{t} = t\omega_p, \quad \varphi = \Phi/\Phi_0 ,$$

to get the normalized 2D inhomogeneous perturbed sine-Gordon equation

$$(2.6) \quad \varphi_{\tilde{t}\tilde{t}} - \Delta \varphi + g(\tilde{x}, \tilde{y})(\kappa \varphi_{\tilde{t}\tilde{t}} + \alpha \varphi_{\tilde{t}} + \sin \varphi) = 0$$

where the coefficients α and κ are

$$(2.7) \quad \kappa = \frac{C_j}{C_l} - 1, \quad \alpha = \frac{1}{R} \sqrt{\frac{\Phi_0}{J_c C_l}}.$$

The boundary conditions are

$$(2.8) \quad \varphi_{\tilde{x}}|_{(\tilde{x}=0)} = \tilde{H} + (1-\nu) \frac{\tilde{I}}{2\tilde{w}}, \quad \varphi_{\tilde{x}}|_{(\tilde{x}=\tilde{l})} = \tilde{H} - (1-\nu) \frac{\tilde{I}}{2\tilde{w}},$$

$$(2.9) \quad \varphi_{\tilde{y}}|_{(\tilde{y}=0)} = \nu \frac{\tilde{I}}{2\tilde{l}}, \quad \varphi_{\tilde{y}}|_{(\tilde{y}=\tilde{w})} = -\nu \frac{\tilde{I}}{2\tilde{l}},$$

where

$$(2.10) \quad \tilde{H} = H \frac{\lambda_J d_0}{\Phi_0}, \quad \tilde{I} = I \frac{\mu_0 d_0}{\Phi_0} = \frac{LI}{\Phi_0},$$

and l and w are normalized by λ_J . After this section all tildes will be omitted for simplicity.

2.2. The 1D model. This equation is difficult to analyze and its solutions can only be obtained numerically. In addition most real devices have a width that is much smaller than their length and the junctions are distributed symmetrically so that it is reasonable to reduce the problem to one dimension. To do this we expand φ on transverse Fourier modes

$$(2.11) \quad \varphi(x, y, t) = \frac{\nu\gamma}{2l} \left(y - \frac{w}{2}\right)^2 + \sum_{n=0}^{\infty} \phi_n(x, t) \cos\left(\frac{n\pi y}{w}\right),$$

where $\gamma = I/w$ and the first term takes care of the boundary condition (2.8). After inserting (2.11) into (2.6) and integrating across y we get the evolution of ϕ_0

$$(2.12) \quad \phi_{tt} - \phi_{xx} + \frac{w_j}{w} g(x, y=0) (\kappa \phi_{tt} + \alpha \phi_t + \sin \phi) = \nu \frac{\gamma}{l},$$

where we omitted the 0 in ϕ_0 and terms in $\phi_i, i \geq 1$ which are small because of the smallness of the current [17].

The boundary conditions are

$$(2.13) \quad \phi_x|_{x=0} = H - (1-\nu) \frac{\gamma}{2}, \quad \phi_x|_{x=l} = H + (1-\nu) \frac{\gamma}{2},$$

and

$$g(x) = \begin{cases} \frac{w_j}{w}, & a_j - \frac{l_j}{2} < x < a_j + \frac{l_j}{2}, \\ 0, & \text{elsewhere.} \end{cases}$$

The factor w_j/w is exactly the "rescaling" of $\lambda_J (= 1)$ into $\lambda_{eff} = \sqrt{\frac{w}{w_j}} > 1$ due to the presence of the lateral passive region [18].

As the area of the junction is reduced the total super-current is reduced and tends to zero. Small junctions where the phase variation can be neglected and that have a significant supercurrent we introduce the following Dirac distribution model. First define the function $g_h(x)$,

$$g_h(x) = \begin{cases} \frac{w_j}{wh}, & a_j - \frac{hl_j}{2} < x < a_j + \frac{hl_j}{2}, \\ 0, & \text{elsewhere,} \end{cases}$$

notice that $g_1(x) = g(x)$. When the junction widths $w_j \ll \lambda_J$ we can further reduce the problem by neglecting the variation of the phase inside the junctions. We then obtain the Dirac delta function distributed model [15, 16] by making h tend to 0. For an n junctions device,

$$\lim_{h \rightarrow 0} g_h(x) = \sum_{j=1}^n \frac{w_j l_j}{l} \delta(x - a_j).$$

Finally we obtain the $\delta - 1D$ model for the device,

$$(2.14) \quad \phi_{tt} - \phi_{xx} + \sum_{j=1}^n d_j \delta(x - a_j) (\kappa \phi_{tt} + \sin \phi + \alpha \phi_t) = \nu \frac{\gamma}{l},$$

where

$$(2.15) \quad d_j = \frac{w_j l_j}{w}$$

and where the boundary conditions are given by eq.(2.13). This is the main model of the article and we will analyze it in detail.

3. Preliminary analysis. From the Josephson equation (1.1) it can be seen that ϕ_t is a voltage. In experiments this instantaneous voltage is of very high frequency (~ 500 GHz) and can only be detected by making it beat with a well-known source. On the other hand the time average voltage can be measured in a fairly standard way. This current voltage relation (the $I - V$ curve) is a characterization of the device. It is therefore important for the analysis to explain it. We now give some important symmetries of the $I - V$ curve. The first one is the periodicity with respect to the magnetic field H . This is similar to the one obtained in the static case [9].

3.1. Periodicity of the $I - V$ curve with H . The $I - V$ curve of the device modeled by eq.(2.14) and (2.13) depends on the magnetic field H . We denote $I - V|_H$ the $I - V$ curve of the device for the magnetic field H . Let us introduce $l_j = a_{j+1} - a_j$ the distance between two consecutive junctions. Let l_{min} be the smallest distance l_j . We define a harmonic array as a circuit where l_i is a multiple of l_{min} for all i .

Proposition, Periodicity of the device.: For a harmonic circuit, the $I - V|_H$ curve is periodic with a period $2\pi/l_{min}$.

Proof.: Let ϕ be a solution of (2.14) for a current γ and a magnetic field H . We introduce $f(x) = (2\pi/l_{min})(x - a_1)$ and $\psi(x; t) = \phi(x; t) + f(x)$. So ψ verifies

$$(3.1) \quad \phi_{tt} - \phi_{xx} + \sum_{j=1}^n \frac{w_j l_j}{l} \delta(x - a_j) (\kappa \phi_{tt} + \sin(\psi - f) + \alpha \phi_t) = \nu \frac{\gamma}{l},$$

with $\psi_x(0; t) = H + 2\pi/l_i - (1 - \nu)\gamma/2$, and $\psi_x(l; t) = H + 2\pi/l_i + (1 - \nu)\gamma/2$. Since, $f(a_j) = 2k\pi$, $\forall i \in \{1; \dots; n\}$, then ψ is a solution of (2.14) for $H + H_p \equiv H + 2\pi/l_{min}$ and for the same γ .

Conversely, by subtracting f from a solution associated to $H + H_p$ and a current γ , we obtain a solution for H and the same current γ . We have shown that for a given γ and H , if there is a solution, we can find another for $H + 2k\pi/l_{min}$ ($k \in \mathbb{Z}$). We obtain the same $I - V$ curves.

$$(3.2) \quad I - V|_{H+H_p} = I - V|_H.$$

with $H_p = 2\pi/l_{min}$.

In the non harmonic case, if the junctions are set such that $l_j = p_j/q_j$, where p_j and q_j are integers, prime with each other, then $I - V|_H$ is periodic with period H_p such that

$$(3.3) \quad H_p = 2\pi \frac{LCM(q_1; \dots; q_{n-1})}{HCF(p_1; \dots; p_{n-1})},$$

where LCM is the Lowest Common Multiple and HCF the Highest Common Factor. To prove this write $f(x) = H_p(x - a_1)$ and use again the previous argument.

3.2. The high voltage approximation . When the voltage ϕ_t is large, the phase ϕ is rotating fast so that one can write

$$(3.4) \quad \phi(x, t) = Vt + \psi(x, t),$$

where the average

$$(3.5) \quad \langle \psi \rangle \equiv \frac{1}{T} \int_t^{t+T} \psi(x, t') dt' \equiv \phi_v(x).$$

Plugging the ansatz (3.4) into (2.14) and taking the average we get

$$(3.6) \quad \langle \psi_{tt} \rangle - \phi_{vxx} + \sum_{j=1}^n d_j \delta(x - a_j) \\ [\kappa \langle \psi_{tt} \rangle + \langle \sin(Vt) \cos(\psi) \rangle + \langle \cos(Vt) \sin(\psi) \rangle + \alpha \langle \psi_t \rangle + \alpha V] = \gamma.$$

Then if we neglect the nonlinear terms we obtain the static equation, we obtain a new equation such that $\langle \psi_{tt} \rangle = \langle \psi_t \rangle = 0$ is a solution. Thus,

$$(3.7) \quad -\phi_{vxx} + \alpha V \sum_{j=1}^n d_j \delta(x - a_j) = \nu \frac{\gamma}{l},$$

together with the boundary conditions

$$(3.8) \quad \phi_{v_x}|_{x=0} = H - (1 - \nu) \frac{\gamma}{2}, \quad \phi_{v_x}|_{x=l} = H + (1 - \nu) \frac{\gamma}{2}.$$

By integrating the equation (3.7) one sees that this problem has a solution if

$$(3.9) \quad V = \frac{\gamma}{\alpha \sum_j d_j}.$$

Let us write this high voltage solution for a device with many junctions. At each junction $x = a_j$, the phase must be continuous. Integrating equation (3.7) over a neighborhood of a_j and taking the limit of this neighborhood going to zero one gets the jump condition

$$(3.10) \quad -[\phi_{v_x}]_{a_j^-}^{a_j^+} + \alpha V \frac{d_j}{l} = 0.$$

Notice also that outside the junctions, the solution has to be of the form

$$\phi_v(x) = -\nu \frac{\gamma}{2l} x^2 + c_1 x + c_2.$$

It is then natural to build the solution by steps, using a sort of shooting method. To simplify the discussion, let us consider a device with two junctions placed respectively at the positions a_1, a_2 . We write

$$(3.11) \quad \phi_v(x) = \begin{cases} \phi_0(x), & 0 \leq x \leq a_1, \\ \phi_1(x), & a_1 \leq x \leq a_2, \\ \phi_2(x), & a_2 \leq x \leq l. \end{cases}$$

At each junction a_j we have $\phi_{j+1}(a_j) = \phi_j(a_j)$ and

$$\phi_{j+1,x}(a_j^+) - \phi_{j,x}(a_j^-) + \alpha V \frac{d_j}{l} = 0.$$

It is then natural to write

$$(3.12) \quad \phi_0(x) = -\nu \frac{\gamma}{2l} x^2 + \left[H - (1 - \nu) \frac{\gamma}{2} \right] x + C.$$

From the relations at each junction, we infer that

$$(3.13) \quad \begin{aligned} \phi_1(x) &= \phi_0(x) + \gamma \frac{d_1}{d_1 + d_2} (x - a_1), \\ \phi_2(x) &= \phi_1(x) + \gamma \frac{d_2}{d_1 + d_2} (x - a_2). \end{aligned}$$

It can be checked that the right boundary condition for $x = l$ can be verified by this formulation whatever the value of H by choosing γ thanks to eq.(3.9). The function $\phi_v(x)$ defined by the equations (3.12-3.13) is then the solution of the problem (3.7,3.8).

3.3. Simplification of the $\delta - 1D$ model. The static part ϕ_v of the high voltage solution can be used to simplify the formulation of the problem, in particular the boundary conditions. For that we introduce

$$(3.14) \quad \psi(x, t) = \phi(x, t) - \phi_v(x),$$

so that the sine-Gordon equation (2.14) becomes

$$(3.15) \quad \psi_{tt} - \psi_{xx} + \sum_{j=1}^n d_j \delta(x - a_j) \left[\kappa \psi_{tt} + \alpha \psi_t + \sin(\psi + \phi_v) - \frac{\gamma}{\sum_{k=1}^n d_k} \right] = 0,$$

with the homogeneous Neumann boundary conditions

$$(3.16) \quad \psi_x|_{x=0} = 0, \quad \psi_x|_{x=l} = 0.$$

Equation (3.15) now contains for each junction a sine term with an argument that is shifted by $\phi_v(a_j) - \phi_v(a_1)$. When averaging over time we get

$$\langle \phi(a_j) - \phi(a_1) \rangle_t \approx \phi_v(a_j) - \phi_v(a_1).$$

We define Ψ_j as the phase-shift of the junction j

$$(3.17) \quad \Psi_j = \phi_v(a_j) - \phi_v(a_1).$$

By a simple translation, equation (3.15) becomes

$$(3.18) \quad \psi_{tt} - \psi_{xx} + \sum_{j=1}^n d_j \delta(x - a_j) \left[\kappa \psi_{tt} + \alpha \psi_t + \sin(\psi + \Psi_j) - \frac{\gamma}{\sum_{k=1}^n d_k} \right] = 0.$$

The boundary conditions (3.16) are unchanged and $\Psi_1 = 0$.

4. Resonances for an array of point junctions.

4.1. Spectral problem. When the system is on a resonance, the solution is periodic so that it can be written as $\psi(x, t) = e^{i\omega t}\varphi(x)$. In that case the terms $\alpha\psi_t + \gamma/\sum_{k=1}^n d_k$ globally balance each other. The sine term can be averaged out. Therefore to satisfy the equation (3.18) it is necessary that

$$(4.1) \quad \psi_{tt} - \psi_{xx} + \sum_{j=1}^n d_j \delta(x - a_j) \kappa \psi_{tt} = 0,$$

together with the homogeneous Neumann boundary conditions (3.16).

When the capacities per unit area of the junctions and passive regions are equal $\kappa = 0$, so the array resonates on a cosine Fourier mode, see [15, 19].

$$\psi_n(x, t) = e^{i\frac{n\pi t}{l}} \cos\left(\frac{n\pi x}{l}\right).$$

In this description, we have neglected the higher harmonics which decay exponentially as shown by numerical calculations. When $\kappa \neq 0$, the eigenmodes of equation (4.1) differ from $n\pi/l$. To analyze them we substitute $\psi(x, t) = e^{i\omega t}\varphi(x)$ into (4.1) and obtain the following eigenvalue problem

$$(4.2) \quad \varphi_{xx} + \omega^2 \left[1 + \sum_{j=1}^n d_j \delta(x - a_j) \kappa \right] \varphi = 0,$$

together with homogeneous Neumann boundary conditions for φ .

We consider the two junctions case. We will obtain results that can be generalized to an array with $n > 2$ junctions. We introduce for ease of notation $\kappa_j = \kappa d_j$. It is then natural to assume a solution

$$(4.3) \quad \varphi(x) = \begin{cases} A_1 \cos(\omega x), & \text{for } 0 \leq x \leq a_1, \\ A_2 \cos(\omega x) + B_2 \sin(\omega x), & \text{for } a_1 \leq x \leq a_2, \\ A_3 \cos(\omega x) + B_3 \sin(\omega x), & \text{for } a_2 \leq x \leq l, \end{cases}$$

where the form of φ in the first interval was chosen to satisfy the boundary condition at $x = 0$. As usual φ is continuous at the junctions $x = a_j$ and one can see that the jump of the derivative is

$$(4.4) \quad [\varphi_x]_{a_j}^{a_j^+} + \kappa_j \omega^2 \varphi(a_j) = 0.$$

Writing these $2n = 4$ conditions at the junctions and the boundary condition at $x = l$, one obtains a 5th order homogeneous system in A_1, A_2, B_2, A_3, B_3 . The solution is non trivial if the following determinant is zero

$$(4.5) \quad \begin{vmatrix} C_1 & -C_1 & -S_1 & 0 & 0 \\ S_1 & -S_1 + \kappa_1 \omega C_1 & C_1 + \kappa_1 \omega S_1 & 0 & 0 \\ 0 & C_2 & S_2 & -C_2 & -S_2 \\ 0 & S_2 & -C_2 & -S_2 + \kappa_2 \omega C_2 & C_2 + \kappa_2 \omega S_2 \\ 0 & 0 & 0 & -S_l & C_l \end{vmatrix} = 0,$$

where $C_1 = \cos(\omega a_1)$, $S_1 = \sin(\omega a_1)$, $C_2 = \cos(\omega a_2)$, $S_2 = \sin(\omega a_2)$, $C_l = \cos(\omega l)$, $S_l = \sin(\omega l)$. When more junctions are present in the device, the determinant giving the

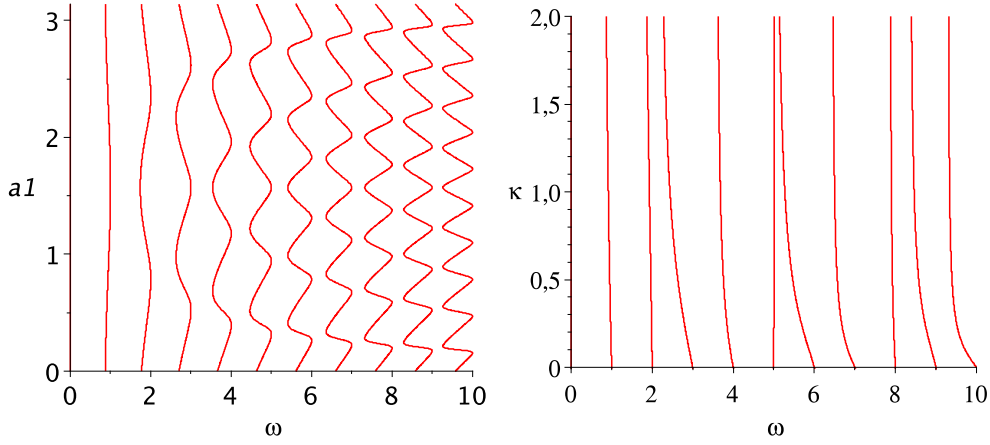


FIG. 4.1. Dependence of the eigenvalues (zeros of the dispersion relation (4.7)) on the position of the junction a_1 in the microstrip (left panel) and on the capacity miss-match κ (right panel). For the left panel, $\kappa = 0.5$. For the right panel $a_1 = 0.3l = 0.3\pi$.

dispersion relation can be generated by adding the elementary component in rows 3 and 4 corresponding to each additional junction.

We now give the resonant frequencies when there is only one junction. The determinant (4.5) becomes

$$(4.6) \quad \left\| \begin{array}{ccc} C_1 & -C_1 & -S_1 \\ S_1 & -S_1 + \kappa_1 \omega C_1 & C_1 + \kappa_1 \omega S_1 \\ 0 & -S_l & C_l \end{array} \right\| = 0,$$

which implies

$$(4.7) \quad \sin(\omega l) + \kappa \omega d_1 \cos(\omega a_1) \cos(\omega(l - a_1)) = 0.$$

Several remarks should be made on this relation.

- First, when $\kappa \ll 1$ we recover the usual $\sin(\omega l) = 0$ dispersion leading to harmonic frequencies.
- The opposite limit $\kappa \gg 1$ is more interesting because it leads to a splitting of the oscillations in the left and in the right side of the film. We obtain $\cos(\omega a_1) = 0$ or $\cos(\omega(l - a_1)) = 0$ leading to $\omega a_1 = (2n + 1)\pi/2$ or $\omega(l - a_1) = (2m + 1)\pi/2$ where m, n are integers.

Notice that Larsen et al [20] considered a centered junction $a_1 = l/2$ in a microstrip. Their dispersion relation

$$\tan \pi \frac{f}{f_e} = -\pi \frac{C_j}{C_e} \frac{f}{f_e},$$

is similar to the one we get with our approach except that the coefficient is different. We obtain using (4.7)

$$(4.8) \quad \tan(\omega l) = -\omega l \left(\frac{C_j}{C_l} - 1 \right) \frac{w_j^2}{\omega l}.$$

This latter expression gives the correct eigenmodes as shown in the current voltage characteristics computed numerically shown in the next sections.

4.2. Eigenvectors and inner product. We introduce here the inner product associated with the dispersion relation (4.7). The eigenvectors φ_i (respectively φ_j) associated to the eigenvalue ω_i (resp. ω_j) satisfy

$$(4.9) \quad \varphi_{i_{xx}} + \omega_i^2 \varphi_i (1 + \delta(x - a_1) \kappa_1) = 0,$$

$$(4.10) \quad \varphi_{j_{xx}} + \omega_j^2 \varphi_j (1 + \delta(x - a_1) \kappa_1) = 0,$$

together with the boundary conditions

$$(4.11) \quad \varphi_{i_x}|_{x \in \{0, l\}} = 0, \quad \text{and} \quad \varphi_{j_x}|_{x \in \{0, l\}} = 0.$$

We assume the eigenvalues to be different. As usual we multiply eq.(4.9) by φ_j and eq.(4.10) by φ_i , subtract the second from the first and integrate on the domain. We obtain

$$(4.12) \quad \int_0^l (\varphi_{i_{xx}} \varphi_j - \varphi_{j_{xx}} \varphi_i) dx + (\omega_i^2 - \omega_j^2) \left[\int_0^l \varphi_i \varphi_j dx + \kappa_1 \varphi_i(a_1) \varphi_j(a_1) \right] = 0.$$

The first integral is zero because of the boundary conditions (4.11). Since $\omega_i \neq \omega_j$ we get

$$(4.13) \quad \int_0^l (1 + \kappa_1 \delta(x - a_1)) \varphi_i \varphi_j dx = 0.$$

Thus we obtain the orthogonality of the eigenvectors φ_i , i is an integer with the associated inner product defined by

$$(4.14) \quad \langle f; g \rangle \equiv \int_0^l (1 + \kappa_1 \delta(x - a_1)) f g dx.$$

It is then possible to normalize the eigenvectors so that they form an orthonormal basis. When there are n junctions in the array, the inner product can be generalized easily to

$$(4.15) \quad \langle f; g \rangle \equiv \int_0^l \left(1 + \sum_{i=1}^n \kappa_i \delta(x - a_i) \right) f g dx.$$

In the case of a single junction, the normalized eigenvectors $\varphi_n(x)$ are given by

$$(4.16) \quad \varphi_n(x) = \begin{cases} A_n \cos(\omega_n x), & \text{for } 0 \leq x \leq a_1, \\ A_n \frac{\cos(\omega_n a_1)}{\cos(\omega_n (l - a_1))} \cos(\omega_n (l - x)), & \text{for } a_1 \leq x \leq l, \end{cases}$$

where ω_n satisfies the dispersion relation (4.7) and

$$(4.17) \quad A_n = \frac{1}{\sqrt{\frac{l}{2} + \frac{\sin 2\omega_n a_1}{4\omega_n} + \frac{\cos^2 \omega_n a_1}{\cos^2 \omega_n (l - a_1)} \frac{\sin 2\omega_n (l - a_1)}{4\omega_n} + \kappa_1 \cos^2 \omega_n a_1}}.$$

Fig. 4.2 shows the 4 non trivial eigenmodes ϕ_i , $i = 1 - 4$ for a large capacity mismatch. Notice how the modes are almost zero on one side of the cavity.

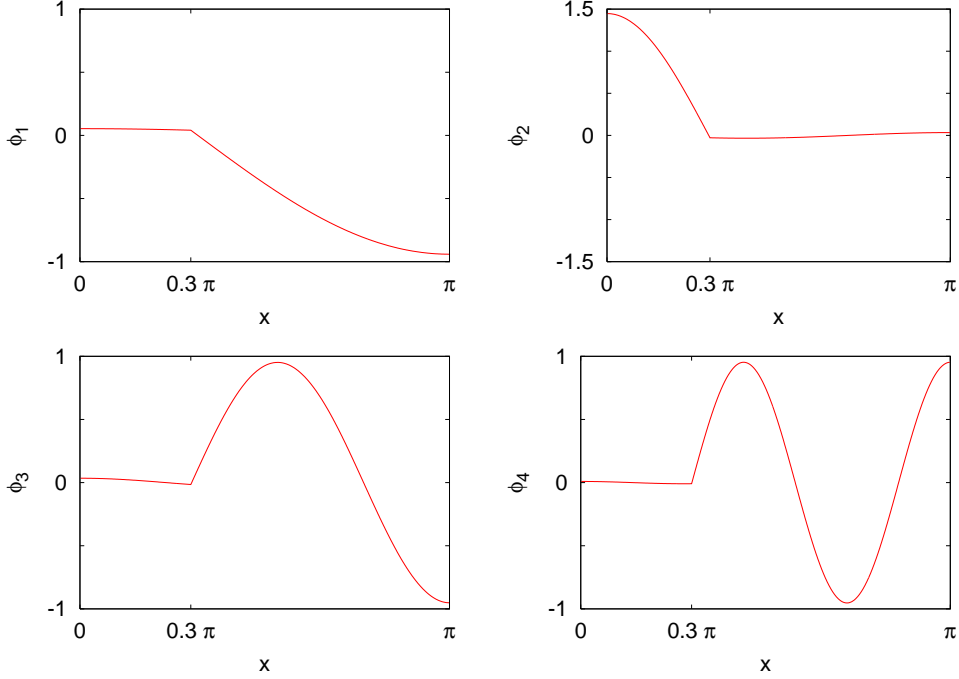


FIG. 4.2. Normalized eigenmodes $\varphi_i(x)$, $i = 1, 2$ (top panels from left to right) and $\phi_i(x)$, $i = 3, 4$ (top panels from left to right) for a large capacity miss-match $\kappa = 30$. The other parameters are $d_1 = 1$, $l = \pi$ and $a_1 = 0.3\pi$.

4.3. Eigenvalues and $I-V$ curves. The eigenvalues calculated in the previous section appear as resonances in the current-voltage characteristics of the device. We computed the $I-V$ curves from the numerical solution of equation (2.14). The singular partial differential equation is integrated over reference volumes and the time advance is done by an ordinary differential equation solver (see Appendix 6 for more details). The average voltage $V \equiv \langle \phi_t \rangle$ is computed over a time interval $10/\alpha$ after waiting a time $100/\alpha$ for the solution to stabilize. When the system is locked on a resonance, it oscillates periodically on an eigenfrequency solution of the dispersion relation eq.(4.7). We will show that the numerical solution follows closely the corresponding eigenvector. We choose a device with $l = \pi$, $a_1 = l/3$, $d_1 = 1$ and take three limiting cases $\kappa = 0$, $\kappa = 1$ and $\kappa = 30$. When there is no capacity miss-match ($\kappa = 0$) we showed in [15] that the resonances of the $I-V$ curve are positioned at $V = k\pi/l$ with k integer and are bounded by

$$\gamma l = d_1 \alpha V, \text{ and } \gamma l = d_1 \sqrt{(\alpha V)^2 + 1}.$$

This is shown in the top panel of Fig. 4.3. In the middle panel we show the $I-V$ curve for $\kappa = 1$. Notice how the resonances are not equally spaced and get sharper. The resonances are very close to the ones given by the dispersion relation, they are reported in table (4.3). Finally on the bottom panel we computed the $I-V$ curve for $\kappa = 30$. This large value is typical in experiments where the oxide layer in the junction is about 100 times thinner than in the passive region. This together with the ratio $d_1 = w_j^2/w$ gives $\kappa_1 \approx 50$. Notice how the resonances are vertical indicating that the system is almost linear. This is to be expected because $\kappa \gg 1$ so that

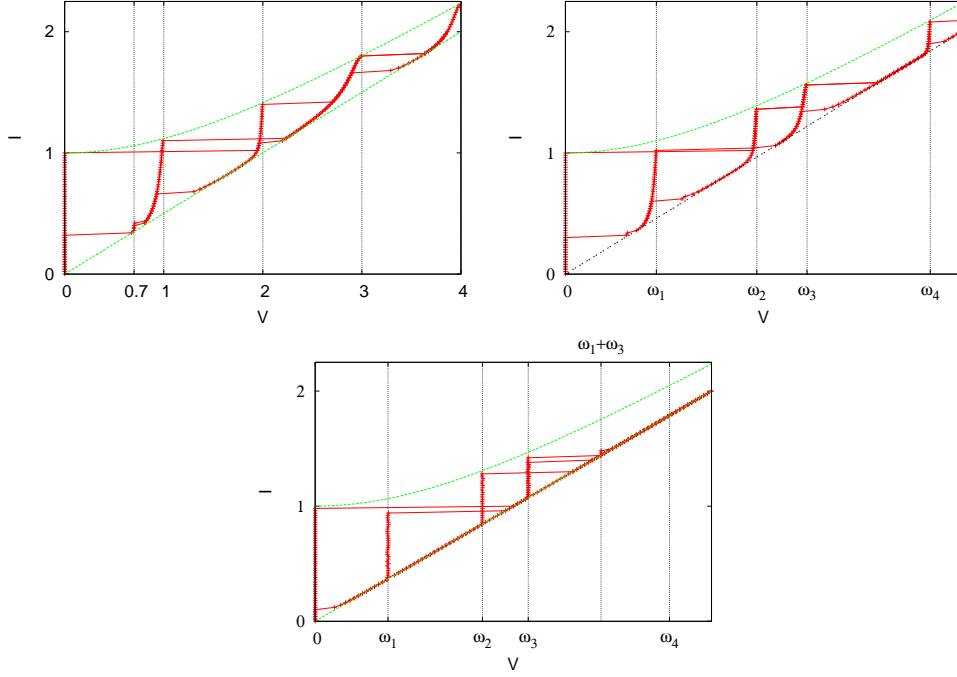


FIG. 4.3. $I - V$ curves for an array with one junction, $d_1 = 1$, $\alpha = 0.5$, $l = \pi$, $a_1 = 0.3\pi$. Top panel, $\kappa = 0$, middle panel $\kappa = 1$ and bottom panel $\kappa = 30$.

i	ω_i	$\cos(\omega_i a)$	Normalization A_i
0	0.	1.	0.491
1	0.917	0.649	0.562
2	1.931	-0.247	1.094
3	2.438	-0.665	0.704
4	3.682	-0.946	0.237

TABLE 4.1
Eigenvalues for the array of Fig. 4.3 with $\kappa = 1$ (middle panel of Fig. 4.3).

the sine term plays little role. The position of the resonances is exactly given by the dispersion relation (4.7). They are reported in the table (4.3) together with the coupling coefficient $\phi_n(a_1)$. The eigenvalues are clearly not harmonic. Notice how some resonances do not go all the way to the junction curve. Another observation is that we have a resonance for ω_2 even though the coupling coefficient is almost zero. We will come back to this point in the next section. Also it is interesting that there is no resonance for ω_4 .

Fig. 4.4 shows the eigenvectors in dashed line (green online) for a realistic value $\kappa_1 = 30$ corresponding to a capacity miss-match $\kappa = 30$ and a surface ratio $d_1 = w_1 l_1/w = 1$. On the same plot are indicated in continuous line (red online) the instantaneous voltages φ_t for different successive times. From top to bottom panels we show respectively the first, second and third resonance. One can see that the

i	ω_i	$\cos(\omega_i a)$	Normalization A_i
0	0.	1.	0.1737
1	0.734	0.770	$5.341 \cdot 10^{-2}$
2	1.687	$-1.950 \cdot 10^{-2}$	1.447
3	2.150	-0.440	$3.462 \cdot 10^{-2}$
4	3.575	-0.974	$9.102 \cdot 10^{-3}$

TABLE 4.2
Eigenvalues for the array of Fig. 4.3 with $\kappa = 30$ (bottom panel of Fig. 4.3).

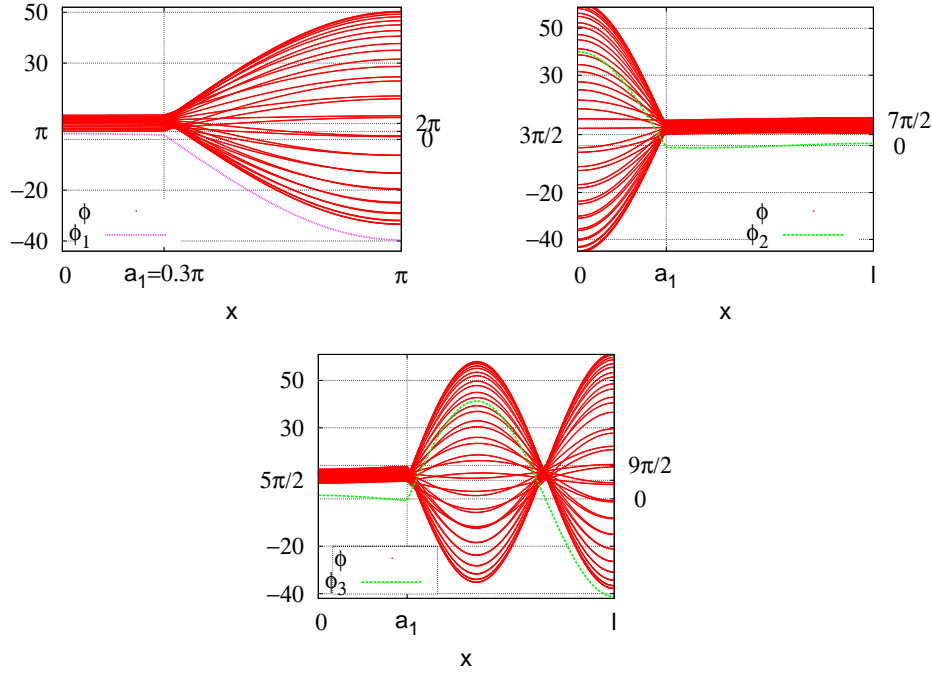


FIG. 4.4. Plot of the instantaneous voltage $\phi_t(x)$ for successive times for the first, second and third resonances in the $I - V$ curve for an array with one junction and with a large capacity miss-match $\kappa_1 = 30$. The corresponding eigenmodes (4.16) are plotted in dashed lines.

voltages follows very well the eigenvectors.

4.4. Projection on the normal modes. The normal modes that we have exhibited can be used to project the solution. This enables to analyze the dynamical behavior in a simple way. The eigenvectors solutions of the problem (4.9) are orthonormal for the inner product defined above. We will assume that all solutions ϕ belong to the vector space generated by the eigenvectors φ_i . This is difficult to justify theoretically but we will come back to this using the numerical results in the last section. Then the solution ψ of equation (3.15) ϕ can be written as

$$(4.18) \quad \psi(x; t) = \sum_{i=0}^{+\infty} \beta_i(t) \varphi_i(x).$$

We assume the uniform convergence of the series (4.18) so that we can permute integrals and sums.

We will present the calculations for a single junction for simplicity. The results can be generalized to arrays with multiple junctions. We replace ψ in eq.(3.15) for one junction,

$$(4.19) \quad \sum_{i=1}^{+\infty} (\beta_i'' \varphi_i - \beta_i \varphi_i'') + d_1 \delta(x - a_1) \left(\sum_{i=1}^{+\infty} (\kappa \beta_i'' \varphi_i + \alpha \beta_i' \varphi_i) + \sin(\psi + \Psi_1) - \frac{\gamma}{d_1} \right) = 0,$$

We multiply eq.(4.19) by $\varphi_j(x)$ and integrate it on its domain

$$(4.20) \quad \sum_{i=1}^{+\infty} \beta_i'' \left(\underbrace{\int_0^l \varphi_i \varphi_j dx + \kappa_1 \varphi_i(a_1) \varphi_j(a_1)}_{=0 \text{ if } i \neq j, =1 \text{ else}} \right) - \beta_i \int_0^l \varphi_i'' \varphi_j dx + d_1 \alpha \beta_i' \varphi_i(a_1) \varphi_j(a_1) + d_1 \sin(\psi(a_1) + \Psi_1) \varphi_j(a_1) - \gamma \varphi_j(a_1) = 0.$$

and from eq.(4.2) we know that,

$$\varphi_i'' = -(1 + \kappa_1 \delta(x - a_1)) \omega_i^2 \varphi_i.$$

Eq.(4.20) becomes

$$(4.21) \quad \beta_j'' + \sum_{i=1}^{+\infty} \beta_i \omega_i^2 \underbrace{\int_0^l (1 + \kappa_1 \delta(x - a_1)) \varphi_i \varphi_j dx}_{=0 \text{ if } i \neq j, =1 \text{ else}} + \frac{d_1 \alpha}{l} \beta_i' \varphi_i(a_1) \varphi_j(a_1) + \frac{d_1}{l} \sin(\psi(a_1) + \Psi_1) \varphi_j(a_1) - \gamma \varphi_j(a_1) = 0.$$

We obtain the final equation giving the evolution of β_j in terms of ϕ

$$(4.22) \quad \beta_j'' + \omega_j^2 \beta_j + c_j \left(\alpha \phi_t(a_1) + \sin(\phi(a_1)) - \frac{\gamma}{d_1} \right) = 0,$$

where we have returned to the usual field ϕ and where the coupling coefficient c_j is

$$(4.23) \quad c_j = d_1 \varphi_j(a_1).$$

This coefficient does not depend directly on κ . Also notice that all equations are coupled by the same term

$$(4.24) \quad F \equiv \alpha \phi_t(a_1) + \sin(\phi(a_1)) - \frac{\gamma}{d_1},$$

where the coefficient c_j regulates the forcing for each mode. When n junctions are present in the device, the modal equations can be generalized to

$$(4.25) \quad \beta_j'' + \omega_j^2 \beta_j + \sum_{k=1}^n c_j^k \left(\alpha \phi_t(a_k) + \sin(\phi(a_k)) - \frac{\gamma}{\sum_{l=1}^n d_l} \right) = 0,$$

where the generalized coupling coefficient c_j^k is

$$(4.26) \quad c_j^k = d_k \varphi_j(a_k).$$

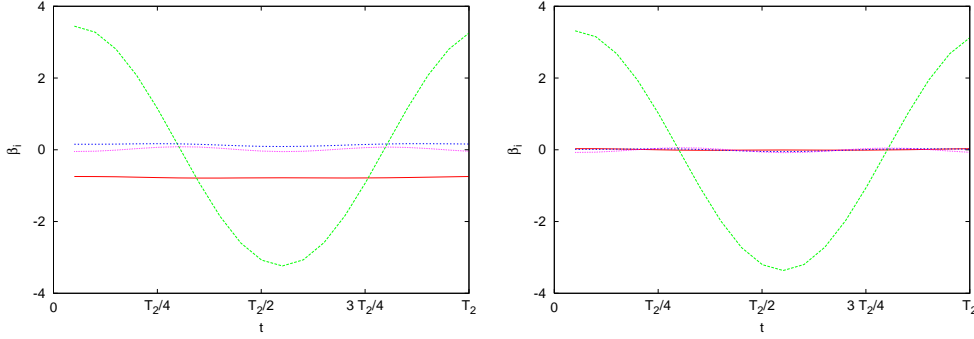


FIG. 5.1. Plot of the amplitudes $\beta_i(t)$, $i = 1 - 4$ obtained by projecting the numerical solution for $\kappa = 1$ at the top of the second resonance onto the normal mode φ_i . The modes are β_1 continuous line, (red online), β_2 dashed line (green online), β_3 short dash (blue online) and β_4 dotted line (pink online). In the left panel the projection is done directly on the solution $\phi(x,t)$. In the right panel we have subtracted the high voltage solution $\phi_v(x)$ for the given current $\gamma = 1.36$. The time unit is the period $T_2 = 2\pi/\omega_2 \approx 3.25$.

5. Numerical analysis of the IV curves. To analyze the mechanism leading to a resonance in the IV curves shown in Fig. 4.3 we project the numerical solution onto the normal modes that we defined in section 4. Following the definition of the inner product (4.14) we have

$$\beta_i = \langle \phi | \phi_i \rangle \equiv \int_0^l \phi \phi_i dx + \kappa d_1 \phi(a_1) \phi_i(a_1).$$

The integral on the right hand side is computed using the trapeze method. Fig. 5.1 shows a plot of the amplitudes β_i , $i = 1 - 4$ for the second resonance with $\kappa = 1$ (middle panel for Fig. 4.3). Clearly β_2 is dominant. In the left panel we did not subtract the high voltage solution $\phi_v(x)$ (3.12-3.13) so that the other modes appear as parasites. If the high voltage solution is taken out then we have a clear dominance of β_2 , all the other modes being close to 0. This shows that we have to a good approximation

$$(5.1) \quad \phi(x,t) \equiv \psi(x,t) + \phi_v(x) \approx \beta_0(t)\varphi_0(x) + \beta_i(t)\varphi_i(x) + \phi_v(x),$$

where $i = 2$ and where we have included the 0 mode that is always present. We recover the results suggested by the plots of Fig. 4.4. We have observed this for all the resonances in the $I - V$ curve. For example for $\kappa = 30$ (bottom panel of Fig. 4.3) we show in Fig. 5.2 the amplitudes β_i from top to bottom for the 1st, 2nd and 3rd resonance. Again the dominant amplitudes are from top to bottom β_1 , β_2 and β_3 .

Therefore the solution at the top of the resonances is given by (5.1) to a good approximation. To analyze how we reach this state we have projected the solution on the normal modes for increasing values of the current γ all the way to the top of the resonance. The calculations were done over a long time interval (about 200 periods). Projecting the solution ϕ we observed a drift in the amplitudes β_i due to the rapid increase of ϕ and the finite precision of the evaluation of the integrals. To avoid these technical problems we have projected the time derivative ϕ_t . The qualitative conclusions are the same as for ϕ except that we will look at $\beta_{i,t}$. Fig. 5.2 shows three amplitudes as a function of time for $\gamma = 1.12, 1.3, 1.42$ and 1.56 and a voltage

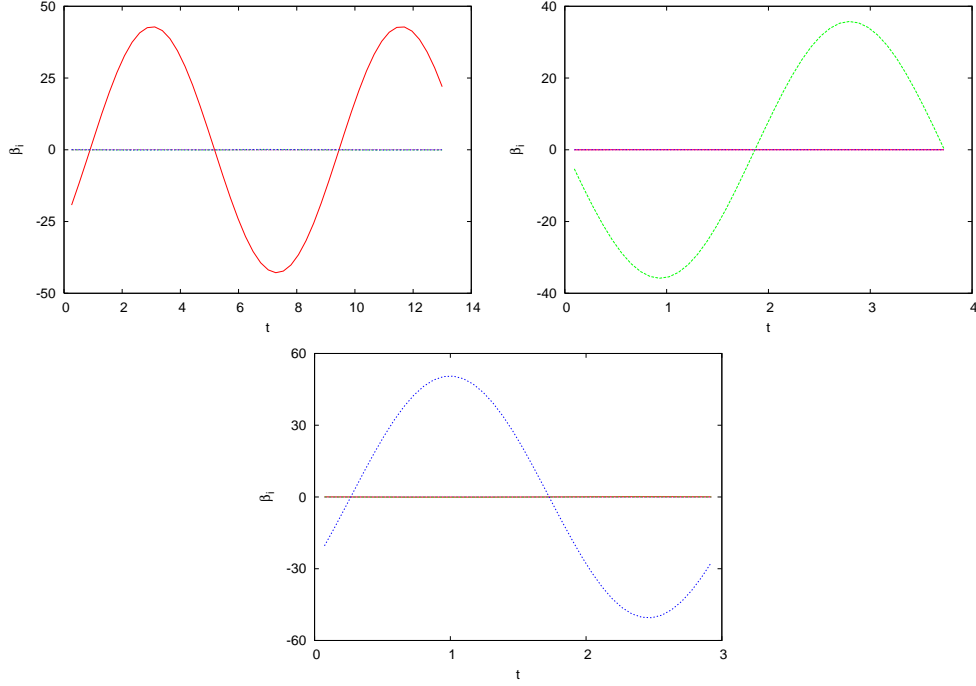


FIG. 5.2. Plot of the amplitudes $\beta_i(t)$, $i = 1 - 3$ obtained by projecting the numerical solution at the top of the second resonance onto the normal mode φ_i for $\kappa = 30$. The dominant mode is resp. $i = 1, 2, 3$ for resp. the 1st resonance (top panel), the second resonance (middle panel) and the third resonance (bottom panel).

$V \approx \omega_3$ near the 3rd resonance for $\kappa = 1$. Only three periods $T_3 = 2\pi/\omega_3$ have been represented for clarity, the rest of the time evolution is the same. In the top left panel for $\gamma = 1.12$, the amplitude of the mode 3 is about 1 with small components in the modes 2 and 1. When the current is increased the amplitude of the 3rd mode increases and becomes periodic of period T_3 . The other modes tend rapidly to 0.

It is instructive to compute numerically the forcing term F as one progresses up the resonance. Fig. 5.4 shows $F(t)$ for three periods T_3 for the four values of γ analyzed in Fig. 5.3. The amplitude of F decreases for increasing γ and F becomes periodic of period T_3 . This explains why we obtain the correct resonant modes using the spectral problem (4.2). Note that when $\kappa = 0$ the forcing term F of the amplitude equations tends to 0 when one gets close to the top of the resonances. Then one can solve the differential equation for $\phi(a_1; t)$

$$(5.2) \quad \alpha \phi'(a_1; t) + \sin(\phi(a_1; t)) - \frac{\gamma}{d_1} = 0,$$

and close the system by expanding this solution using the standard Fourier modes[15]. This is not the case when $\kappa \neq 0$ as shown by these numerical results. To analyze the resonances, we assume as in [12] that when in resonance, the solution has the spatial structure of the corresponding eigenmode.

$$(5.3) \quad \psi(x, t) = \beta_0(t)\varphi_0 + \beta_n(t)\varphi_n(x),$$

where the first term on the right corresponds to the zero mode. The evolution of

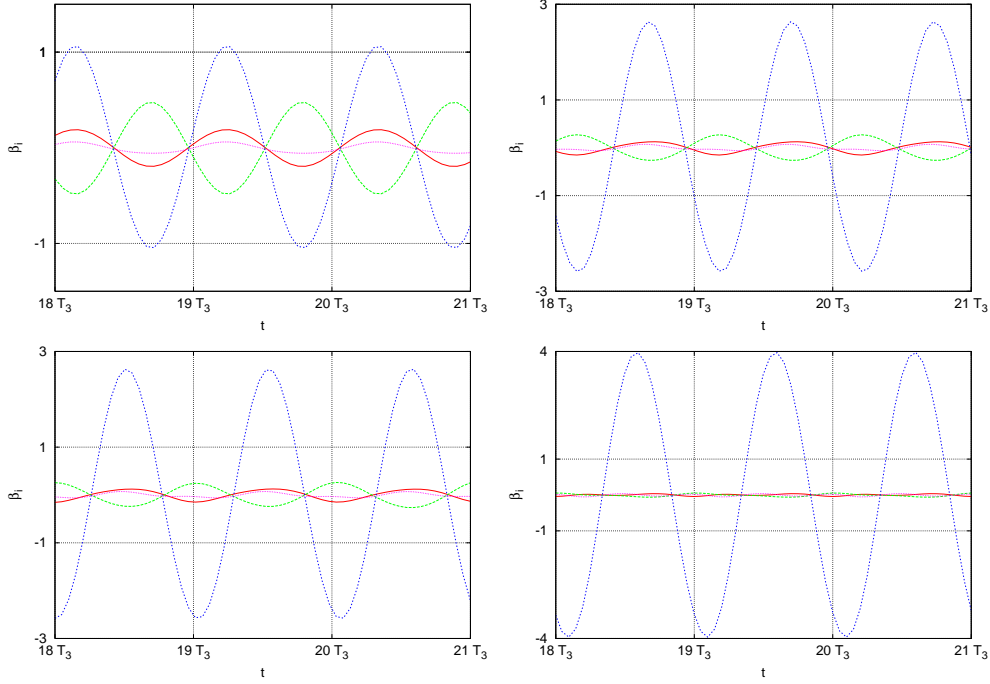


FIG. 5.3. Plot of the amplitudes of $\phi_t(x, t)$ as a function of time for four different values of the current, from top left to bottom right $\gamma = 1.12, 1.3, 1.42, 1.56$, on the third resonance $V = \omega_3$ for $\kappa = 1$. The index of the modes are $i = 1$ continuous (red online), $i = 2$ dashed line (green online), $i = 3$ short dash (blue online) and $i = 4$ dotted line (pink online). The time interval is the period $T_3 = 2\pi/\omega_3 \approx 2.58$.

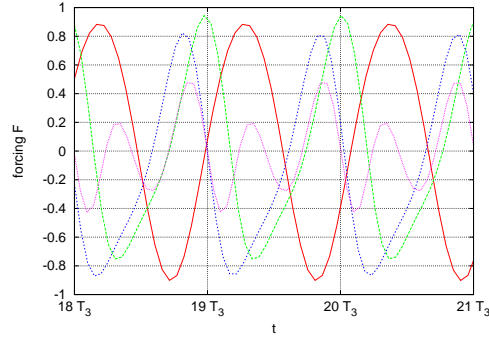


FIG. 5.4. Plot of the forcing term F from (4.24) as a function of time for four different values of the current on the third resonance $V = \omega_3$ for $\kappa = 1$. The values are $\gamma = 1.12$ continuous (red online), $\gamma = 1.3$ dashed line (green online), $\gamma = 1.42$ short dash (blue online) and $\gamma = 1.56$ dotted line (pink online). The time interval is the period $T_3 = 2\pi/\omega_3 \approx 2.58$.

β_0, β_n is then given by equation (4.22)

$$(5.4) \quad \beta_n'' + \omega_n^2 \beta_n + c_n F = 0,$$

$$(5.5) \quad \beta_0'' + c_0 F = 0,$$

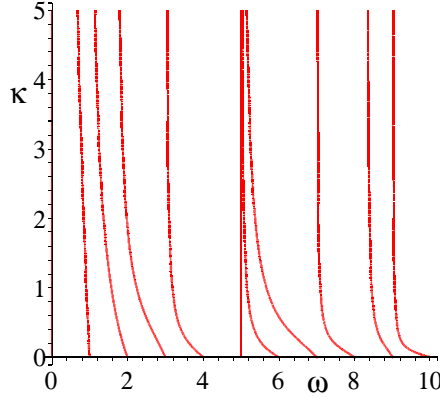


FIG. 5.5. Plot of the frequency ω vs. κ_i for a device with two junctions where $a_1 = 0.3\pi$, $a_2 = 0.5\pi$, $d_1 = d_2 = 0.1$.

where the forcing term is

$$(5.6) \quad F = \alpha\beta'_n\varphi_n + \alpha\beta'_0\varphi_0 + \sin(\beta_n\varphi_n + \beta_0\varphi_0) - \frac{\gamma}{d_1}$$

To understand the specific shape of the resonances, the fact that we cannot obtain in the IV curve the right part of the resonance curve, one could carry out a bifurcation analysis similar to the one of [21]. However this is out of the scope of this article.

The situation is more complex when there are more junctions in the device. As an example we consider a two junction device with $l = \pi$, $a_1 = 0.3\pi$, $a_2 = 0.5\pi$, $d_1 = d_2 = 0.1$. The eigenmodes ω_n are plotted in Fig. 5.5 as a function of κ and one can see them shift from integer values even for small κ . In Fig. 5.6 we plot the $I - V$ curves obtained for this device for $\kappa = 0, 4$ and 8 with $d_1 = 0.1$ so that $\kappa_1 = d_1\kappa = 0, 0.4$ and 0.8 . The resonances observed correspond to the eigenfrequencies obtained. For $\kappa = 0$ we have explained the height of the resonances using an approximate theory [19] based on the amplitude of oscillation of $\phi_i(a_j)$ for each junction. This is the envelope function plotted in dashed line in the top left panel of Fig. 5.6. When $\kappa \geq 0$ it is more difficult. We think that this amplitude of oscillation, which can be obtained by the eigenvectors does not determine completely the height of the resonances. When the length of the device is larger more resonances can be accommodated in the $I - V$ curve. An interesting effect we found is that for large values of κ the system locks to linear combinations of the eigenfrequencies. Such an example is shown in Fig. 5 for a two junction device in a microstrip of length $l = 10$. For $\kappa \geq 5$ there appears in the $I - V$ curve a resonance for $\omega_1 + \omega_6$. For $\kappa = 10$ (bottom left panel) we see in addition resonances for $2\omega_1$, $\omega_1 + \omega_9$. This is typical of a linear system. When we observe numerically the evolution of ϕ_t at this resonance we see the two eigenvectors 1 and 9. But we cannot explain this linear behavior: how the system can sum two non linear solution?

5.1. Conclusion. To summarize we have analyzed a long wave model describing a parallel array of Josephson junctions. We defined an appropriate spectral problem whose spectrum gives the resonances of any array with junctions of arbitrary (small) sizes and positions. This task would not have been possible without the complexity

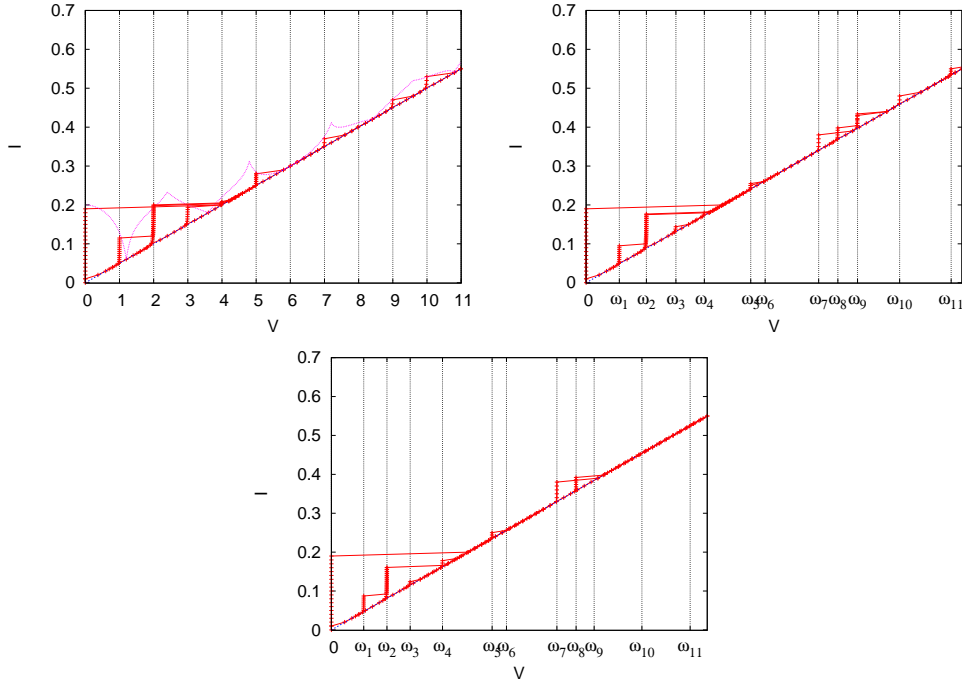


FIG. 5.6. I - V curves for the two junction circuit studied in Fig. 5.5. The parameters are $l = \pi$, $d_1 = d_2 = 0.1$, $\alpha = 0.25$, $\kappa = 0$. From top left to bottom $\kappa = 0, 4$ and 8 . In the top panel the envelope function (see text) is plotted as a dashed line (pink online).

reduction provided by asymptotic analysis.

The adapted spectral problem leads to an inner product so that it becomes possible to project the dynamics of the system and describe arrays with more junctions.

It may now be possible to solve the inverse problem of finding the device yielding a given I - V curve. Another open question is the study of the amplitude equations (5.4) to analyze the stability of the resonances.

Acknowledgements

J.G.C. and L. L. thank Faouzi Boussaha and Morvan Salez for helpful discussions and for their experimental results. The computations were done at the Centre de Ressources Informatiques de Haute-Normandie (CRIHAN).

REFERENCES

- [1] B. D. Josephson, Phys. Lett. **1**, 251, (1962).
- [2] A. Barone and G. Paterno, *Physics and Applications of the Josephson effect*, J. Wiley, (1982).
- [3] K. Likharev, *Dynamics of Josephson junctions and circuits*, Gordon and Breach, (1986).
- [4] M. SALEZ ET AL., Proc. SPIE Conf. on Telescopes and Astronomical Instrumentation, Hawaii, 2002 (August 22-28), col. 4855, p. 402, Proc. 4th European Conference on applied superconductivity, EUCAS 99, 651, (1999)
- [5] F. BOUSSAHA ET AL., *Fundamental and harmonic submillimeter-wave emission from parallel Josephson junction arrays*, J. of Applied Physics 105, 073902, (2009).
- [6] B. VASILIC, P. BARBARA, S. V. SHITOV AND C. J. LOBB Phys. Rev. B, 65, 180503(R), (2002).
- [7] J. G. CAPUTO, N. FLYTZANIS AND M. VAVALIS, *A semi-linear elliptic pde model for the static solution of Josephson junctions*, International Journal of Modern Physics C, vol. 6, No. 2, 241-262, (1995).

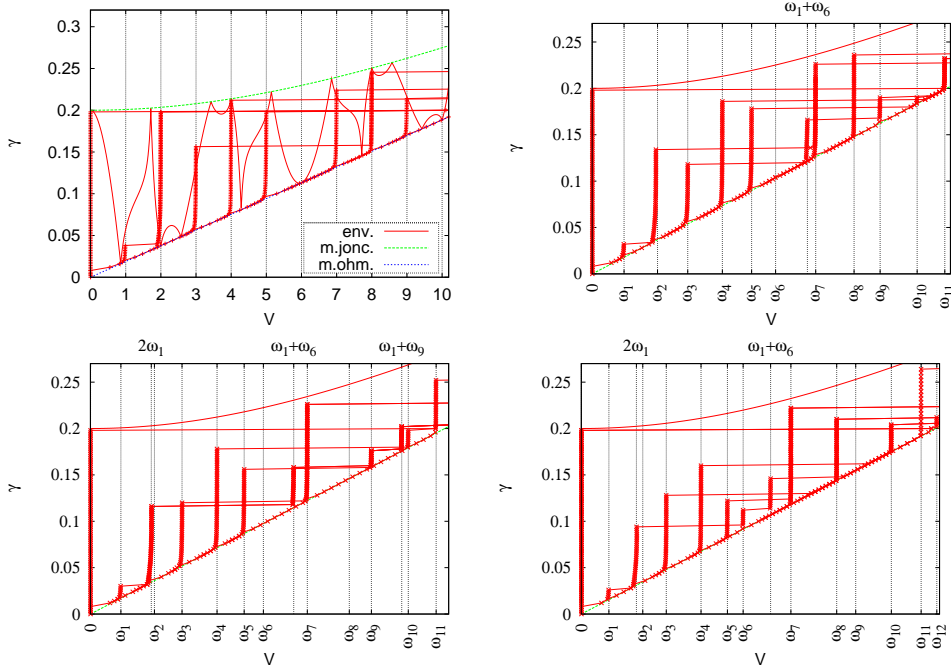


FIG. 5.7. $I-V$ curves of a two junction device, $a_1 = 10/3$, $a_2 = 25/3$, $l = 10$, $d_i = 0.1$, $\alpha = 0.3$ and different values of κ . Top panels, $\kappa = 0$ (left) and $\kappa = 5$ (right). Bottom panels $\kappa = 10$ (left) and $\kappa = 22$ (right).

- [8] J. G. CAPUTO, N. FLYTZANIS, A. TERSENOV AND M. VAVALIS, *Analysis of a semi-linear pde for modeling static solutions of Josephson junctions*, SIAM J. of Math. Analysis, **34**, 1356-1379, (2003).
- [9] J. G. CAPUTO AND L. LOUKITCH, *Statics of point Josephson junctions in a micro strip line*, SIAM J. Appl Math, **67**, No. 3, 810-836, (2007).
- [10] M. SALEZ, F. BOUSSAHA, L. LOUKITCH AND J. G. CAPUTO, *Interference filter properties of nonuniform Josephson junction arrays*, J. Appl. Phys. **102**, 083904, (2007).
- [11] J. G. CAPUTO AND L. LOUKITCH, *Designing arrays of Josephson junctions for specific static responses*, Inverse Problems 24 No 2 (April 2008), 025022.
- [12] I. O. Kulik, Soviet Physics-Technical physics, vol. 12, 1, 111-116, (1967).
- [13] M. CIRILLO, N. GRONBECH-JENSEN, M. R. SAMUELSEN, M. SALERNO AND G. VERONA RINATI, *Fiske modes and Eck steps in long Josephson junctions: theory and experiments*, Phys. Rev. B, **58**, 12377, (1998).
- [14] J. PFEIFFER, A. A. ABDUMALIKOV JR., M. SCHUSTER AND A. V. USTINOV, *Resonances between fluxons and plasma waves in underdamped Josephson transmission lines of stripline geometry*, Phys. Rev. B, **77**, 024511, (2008).
- [15] J. G. CAPUTO AND L. LOUKITCH, *Dynamics of point Josephson junctions in microstrip line.*, Physica **425** (2005) 69-89.
- [16] L. Loukitch, *Modélisation et analyse mathématique d'un système à non-linéarités distribuées: les réseaux hétérogènes de jonctions Josephson*, PhD thesis, INSA de Rouen, December 2006.
- [17] A. Benabdallah, J. G. Caputo and N. Flytzanis, Physica D **161**, 79-101, (2002)
- [18] J. G. Caputo, N. Flytzanis and M. Vavalis, *Effect of geometry on fluxon width in a Josephson junction*, Journal of Modern Physics C, vol. 7, No. 2, 191-216, (1996).
- [19] J. G. Caputo and L. Loukitch, *A system with distributed nonlinearities: the array of Josephson junctions*, "Nonlinear waves in complex systems: energy flow and geometry", Collection "Special Topics" of European J. Phys. **147**, (1), (2007).
- [20] A. Larsen, H. Dalsgaard Jensen, J. Mygind, Phys. Rev. B, vol. 43, 10179-10190, (1991).
- [21] D. L. Brown, M. G. Forest, B. J. Miller and N. A. Petersson, *Computation and stability of*

fluxons in a singularly perturbed sine-Gordon model of the Josephson junction, Siam J. Appl. Math, **54**, 1048-1066, (1994).

- [22] E. HAIRER, S. P. NORSETT AND G. WANNER. *Solving ordinary differential equations I*, Springer-Verlag, (1987).

6. Appendix. The basis of the method is to discretize the spatial part of the operator and keep the temporal part as such. We thereby transform the partial differential equation into a system of ordinary differential equations. This method allows to increase the precision of the approximation in time and space independently and easily. In our case the operator is a distribution so that the natural way to give it meaning is to integrate it over a volume. We therefore choose as space discretisation the finite volume approximation where the operator is integrated over reference volumes. The value of the function is assumed constant in each volume. As solver for the system of differential equations, we use the Runge-Kutta method of order 4-5 introduced by Dormand and Prince implemented as the Fortran code DOPRI5 by Hairer and Norsett [22] which enables to control the local error by varying the time-step.

We first transform (..) into a system of first order partial differential equations We write $\psi(x, t) = \phi_t(x, t)$.

$$(6.1) \quad \begin{cases} \psi(x, t) &= \phi_t(x, t) \\ \psi_t(x, t) &= \phi_{xx}(x, t) - \delta(x - a)(\kappa\psi_t(x, t) + \alpha\psi(x, t)) + d_1 \sin(\phi(x, t)) + \nu\gamma/l \end{cases}$$

with the boundary conditions : $\phi_x|_{\frac{l}{2}} = H - (1 - \nu)\gamma/2$, and $\phi_x|_{-\frac{l}{2}} = H + (1 - \nu)\gamma/2$.

For simplicity we will describe the implementation of the finite volume discretisation in the case of a single junction. We introduce reference volumes V_k whose centers we call x_k , $1 \leq k \leq nn$. The discretisation points are placed such that the point x_{ng+1} is at the junction, ($x_{ng+1} = a$). We thus define x_k and V_k using the following identities

$$V_k = \left] x_k - \frac{h_g}{2}, x_k + \frac{h_g}{2} \right[, \quad 0 < k < ng + 1$$

with $(ng + 1)h_g = a$

$$V_k = \left] x_k - \frac{h_d}{2}, x_k + \frac{h_d}{2} \right[, \quad ng + 1 < k < nn + 1$$

with $(nn - ng)h_d = l - a$. Finally at the junction, $k = ng + 1$

$$V_{k_{ng+1}} = \left] x_{ng+1} - \frac{h_g}{2}, x_{ng+1} + \frac{h_d}{2} \right[.$$

nn , ng and nd are respectively the total number of discretisation points, the number of points to the left of the junction and the number of points to the right.

For a fixed t , we assume $\phi(x, t)$ to be constant on each volume V_k , so that

$$\int_{x_k - \frac{h}{2}}^{x_k + \frac{h}{2}} \phi(x, t) dx = h\phi(x_k, t) , \quad \text{with } h = h_g \text{ or } h = h_d$$

Integrating over V_k yields:

In the linear part of the partial differential equation : $0 < k < nn + 1$ and $k \neq ng + 1$:

$$(6.2) \quad \begin{cases} \psi(x_k, t) &= \phi_t(x_k, t) \\ \psi_t(x_k, t) &= \frac{\phi(x_{k+1}, t) - 2\phi(x_k, t) + \phi(x_{k-1}, t))}{h^2} + j \end{cases}$$

with $h = hg$ for $0 < k < ng + 1$ or $h = hd$ for $k > ng + 1$. We recognize the usual discretisation of the second derivative.

At the junction: $k = ng + 1$, we obtain

$$\int_{x_{ng+1}-\frac{hg}{2}}^{x_{ng+1}+\frac{hd}{2}} \delta(x-a) (\kappa\phi_{tt}(x,t) + \alpha\phi_t(x,t) + d_1 \sin(\phi(x,t))) =$$

$$d_1 \sin(\phi(x_{ng+1}, t)) + \alpha\phi_t(x_{ng+1}, t)$$

So that the final system is:

$$\psi(x_{ng+1}, t) = \phi_t(x_{ng+1}, t)$$

$$\psi_t(x_{ng+1}, t) = \left[\frac{4}{hg + hd} \left(\frac{\phi(x_{ng+2}, t) - \phi(x_{ng+1}, t)}{hg/2} - \frac{\phi(x_{ng+1}, t) - \phi(x_{ng}, t)}{hd/2} \right) \right. \\ \left. - \frac{2}{hg + hd} (d_1 \sin(\phi(x_{ng+1}, t)) + \alpha\phi_t(x_{ng+1}, t)) + j \right] \frac{1}{1 - d_k \kappa}$$

The previous system of ordinary differential equations is then integrated numerically using the DOPRI5 integrator.